Effects of polyethylene fibre dosage and length on the properties of high-tensile-strength engineered geopolymer composite

Jia-Qi Wu[a]

[a] Department of Civil Engineering, University of Nottingham Ningbo China, Taikang Road, Ningbo, China.

jiaqi.wu@nottingham.edu.cn

Bo Li[a,b,*]

[a] Department of Civil Engineering, University of Nottingham Ningbo China, Taikang Road, Ningbo, China.

[b] New Materials Institute, University of Nottingham Ningbo China, Taikang Road, Ningbo, China.

[*] Corresponding author: bo.li@nottingham.edu.cn

Yung-Tsang Chen[a]

[a] Department of Civil Engineering, University of Nottingham Ningbo China, Taikang Road, Ningbo, China.

yung-tsang.chen@nottingham.edu.cn

Bahman Ghiassi[c]

[c] School of Engineering, University of Birmingham, Birmingham, United Kingdom.

b.ghiassi@bham.ac.uk

Ahmed Elamin[d]

[d] School of Engineering, University of Greenwich, Greenwich, London, United Kingdom.

ahmed.elamin@gre.ac.uk

Abstract

This paper presents a high-tensile-strength Engineered Geopolymer Composite (EGC) reinforced by polyethylene (PE) fibres. The influences of fibre dosage (1.5%, 1.75% and 2.0%) and length (6 mm, 12 mm and 18 mm) on the mechanical properties and straining hardening performance of EGCs were examined. The results indicate that increasing either fibre dosage or length decreases the flowability of EGC due to the skeleton formed by fibres. The increase of fibre dosage from 1.5% to 2.0% enhances the fibre bridging effect in the EGCs with 12 mm PE fibres and subsequently enhances their compressive and tensile strengths by 9.0% and 12.7%, respectively. Differently, the increase of 18 mm fibre dosage from 1.5% to 2.0% introduces more voids inside the EGCs, which decreases their compressive and tensile strengths by 3.8% and 3.6%, respectively. Fibre cluster is more likely to occur in EGC with a higher dosage of longer fibres, which reduces its tensile strength. A higher fibre dosage improves both tensile strain capacity and crack control capacity of EGC. On the other hand, increasing the fibre length from 6 mm to 18 mm increases the tensile strength by 42.0%, strain capacity by 148.0%, and crack control ability of EGC by enhancing the fibre bridging effect, although it is detrimental to the compressive strength of the EGCs with 18 mm fibres due to the magnified air entrapping effect. In addition, a prediction model modified based on the test results can accurately predict the tensile strength of PE fibre reinforced EGCs. The environmental assessment indicates developed EGCs exhibit dramatically lower environmental impacts than the conventional engineered cementitious composite.

Keywords: Engineered geopolymer composite; alkali activation; slag-fly ash blends; high tensile strain capacity; polyethylene fibre

1 Introduction

Engineered Cementitious Composites (ECCs) are a family of fibre-reinforced cementitious materials which are famous for their high tensile strength and strain capacity (Li 2019; Li and Leung 1992). For example, the tensile strength and strain capacity of the conventional M45 ECC can reach 5.9 MPa and 2.7%, respectively (Yang et al. 2007). These characteristics are beneficial to enhancing the durability and resiliency of the infrastructures constructed with ECC (Wu et al. 2021; Huang et al. 2020). To achieve the superior tensile properties, ECCs are normally prepared with a large amount of cement, a low water-to-binder ratio, the incorporation of fine aggregate, the use of ultra-highmolecular-weight polyethylene (PE) fibres (Zhang et al. 2020), and the surface treatment to reduce the hydrophobicity of PE fibre (Wu and Li 1999; He et al. 2017). However, the high cement content and superplasticiser dosage sacrifice the sustainability of ECC in terms of carbon emission and energy consumption. Damtoft *et al.* (2008) reported that the cement production emits 5-8% of the total carbon dioxide worldwide, and producing one ton of cement emits around 0.87 tons of carbon dioxide. Meanwhile, most superplasticisers used in concrete are not biodegradable (Yang et al. 2019), and the production of polycarboxylate superplasticiser commonly used in high-performance concrete also consumes a large amount of energy (Liu et al. 2021). This necessitates the development of alternative binder to ordinary Portland cement for enhancing the sustainability of ECC.

To improve the sustainability of ECC, geopolymer has been proposed as an alternative binder through activation of waste materials or industrial by-products. The new type of fibre-reinforced geopolymer composite, also named as Engineered Geopolymer Composite (EGC), has attracted great attention due to its environmental benefits and superior mechanical properties (Lyu et al. 2021). Nevertheless, Nath *et al.* (2015) pointed out that the strength development of geopolymer prepared with fly ash as a sole precursor is very slow at ambient temperature (23ºC), and the mixture even exhibits insufficient compressive strength at the age of 3 days. Although high-temperature curing can be adopted to accelerate and enhance geopolymerisation (Rovnaník 2010), this curing method also increases the energy consumption in the production of geopolymer and requires a special curing facility in practice, which eventually limits the applications of geopolymer in the construction industry. To overcome this shortcoming, ground granulated blast-furnace slag (GGBS), a type of calcium-rich material, is usually added into fly ash based geopolymer to enhance its early strength by forming calcium aluminosilicate hydrate (C-A-S-H) and densifies the microstructure of composite (Rafeet et al. 2019). Therefore, alkali-activated fly ash/GGBS blends are able to achieve sufficient strength as the matrix of ambient-cured EGC.

Alkali-activated fly ash/GGBS has been successfully utilised as the matrix of ambient-cured EGCs reinforced by Polyvinyl alcohol (PVA) fibres. Farooq *et al.* (2020) investigated the properties of PVA fibre-reinforced EGCs cured at ambient temperature, and found that the EGCs using alkaliactivated fly ash/GGBS blends as matrix achieve a tensile strength of 3-5 MPa and a tensile strain capacity of 1.5-3%. Zhong and Zhang (2021) also studied the effect of PVA fibre dosage on the performance of EGCs cured at ambient temperature, and reported that the tensile strength and tensile strain capacity of the EGC reinforced by 2% of PVA fibres are around 3.7 MPa and 4.0%, respectively. Similarly, Wang *et al.* (2022) proposed an ambient-cured EGC with a tensile strength of 4.45% and a tensile strain capacity of 4.91% when 2% of PVA fibres are incorporated. Considering the fibrereinforced composites with strain-hardening behaviour are generally utilised in shear (Wei et al. 2020) or tension zones (Huang et al. 2019) of structural members, both tensile strength and strain capacity are essential for EGCs to fulfil their functions. Hence, the proper selection of fibre reinforcement is crucial to achieve an excellent tensile performance of EGC.

To improve the tensile performance of ambient-cured EGCs, PE fibres have been recognised as suitable reinforcement in composites. They have been proven as excellent reinforcement to achieve high tensile strength and strain capacity in ECC (Yu et al. 2018; Curosu et al. 2017). Shaikh *et al.* (2018) reported that the ambient-cured EGC reinforced by 1% of PE fibres can achieve a tensile strength of 4 MPa and a tensile strain capacity of 6%. Alrefaei and Dai (2018) investigated the tensile behaviour of one-part EGCs reinforced by hybrid fibres (i.e., steel and PE fibres) cured at ambient temperature, and found that the EGCs with hybridized fibres possess a tensile strength of 3.25-3.43 MPa and a tensile strain capacity of 4%. Moreover, the amount of PE fibres plays a key role in determining the tensile strain capacity of EGC. Kan and Wang (2021) reported that the tensile strength and tensile strain of alkali-activated composites with 1.9% of 12 mm PE fibres can reach 4.9 MPa and 1.9%, respectively. Nematollahi *et al*. (2017b) also found the tensile strength and tensile strain capacity of one-part geopolymer composite with 2% 12 mm PE fibres are 4.2 MPa and 5.5%, respectively. However, tensile performance of ambient-cured EGCs with PE fibres can be further enhanced as compared with that of PE fibre reinforced ECCs, which can be optimized through tailoring their PE fibre length and dosages.

PE fibres have been utilised to produce high performance fibre-reinforced alkali-activated materials. However, the selection of PE fibre reinforcement in terms of dosage and length still needs to be further studied. Choi *et al.* (2016a) reported that the alkali-activated slag-based composite with

1.75% of 18 mm PE fibres can achieve a tensile strength of 13 MPa and a tensile strain capacity of 7.5%. Choi *et al.* (2016b) utilised 1.75% of 12 mm PE fibres to reinforce alkali-activated slag composite which attains a tensile strength of 7.89 MPa and a tensile strain of 5.32%. Luong *et al.* (2021) developed a sustainable alkali-activated slag-based composite reinforced by 1.75% of 18 mm PE fibres, and found the composite with 10% crumb rubber particles attains a tensile strength of 9.5 MPa and a tensile strain of 10.6%. Kumar *et al.* (2022) found that the EGC with 1.5% of 18 mm PE fibres and 0.5% of steel fibres exhibits a tensile strength of 6.24 MPa and a tensile strain capacity of 5.60%. The above-mentioned studies demonstrate that the optimum PE fibre dosage and length adopted to achieve superior tensile performance of EGC remain debatable. In particular, the efficiency of PE fibre bridging effect in EGC might be affected by the fibre length and dosage. Therefore, it is necessary to perform a systematic study focusing on the influences of PE fibre length and dosage on the performance of EGC.

This paper aims to develop a high-tensile-strength and high-tensile-strain capacity PE fibre reinforced engineered geopolymer composite cured at ambient temperature. The influences of PE fibre length (6 mm, 12 mm and 18 mm) and dosage (1.5%, 1.75% and 2%) on the performance of high-tensile-strength engineered geopolymer composites, including flowability, density, compressive strength, tensile performance, and cracking behaviour, are systematically investigated. The efficiency of PE fibre reinforcement in affecting the tensile performance is estimated, and a modified prediction model is proposed to predict the tensile strength of PE fibre reinforced EGCs. Scanning Electronic Microscope (SEM) analysis is also utilised to characterise the failure mode of fibres and the microstructure at the fibre-to-matrix interfaces in the developed EGCs. Besides, the environmental impacts of developed EGCs cured at ambient temperature are compared with those of conventional ECC based on the material sustainability indicators (MSIs).

2 Materials and Methods

2.1 Raw materials

Low-calcium fly ash and Ground Granulated Blast-furnace Slag were adopted as the precursors of geopolymer. Their compositions detected by X-ray fluorescence (XRF) are listed in **Table 1**, and their particle size distributions measured by a laser particle size analyser are plotted in **Fig. 1**. The alkaline activator was prepared by blending sodium hydroxide pellets (analytical grade, ≥96 wt% purity), sodium silicate solution (Na_2O = 8.32%, SiO_2 = 26.83% and H_2O = 64.85%), and water. To achieve proper flowability and setting time of EGCs, the alkali dosage (i.e., Na_2O/binder mass ratio) and the silicate modulus (SiO_2/Na_2O molar ratio) were set as 4.5% and 2.25, respectively. The NaOH pellets were first dissolved into the water and then blended with the sodium silicate solution. The activator solution was cooled to ambient temperature before it was used for preparing geopolymer (Rafeet et al. 2019). In addition, fine silica sand with a maximum size of 250 μm and a mean size of 100 μm was used as the aggregate in EGCs. PE fibre with a diameter of 24 μm and three different lengths (6 mm, 12 mm and 18 mm) were used as the reinforcement in EGCs as shown in **Fig. 2**. The Young's modulus and tensile strength of PE fibre are 110 GPa and 3000 MPa, respectively. The elongation of PE fibre at fracture is 2-3%.

2.2 Mix proportions

The mix proportions of the EGCs are summarised in **Table 2**. Based on the trial tests and the study by Huang *et al*. (2021c), the water-to-binder ratio and sand-to-binder ratio of the EGCs were fixed at 0.33 and 0.3, respectively. The PE fibre length (6 mm, 12 mm, and 18 mm) and dosage (1.5%, 1.75%, and 2.0% by volume) are the control parameters in the test. In the Mix ID, the first number represents the length of PE fibre, and the second percentile means the volume fraction of PE fibres. A mix without PE fibre reinforcement (denoted as 'Mortar') was also prepared for comparison.

2.3 Sample preparation and test procedures

Mixture preparation and curing. The dry powders, including the binder and the silica sand, were first mixed for 2 minutes, followed by adding alkaline activator and mixing for another 5 minutes to produce a homogenous geopolymer mortar. Afterwards, the PE fibres were continuously added into the mortar, and the EGCs were mixed for another 3 minutes to ensure the uniform dispersion of fibres. After casting, the samples were covered by a plastic film to prevent moisture loss till demoulding (around 24 h). The demoulded samples were sealed by a plastic film and transferred to a curing chamber with a temperature of 23 ± 2ºC and a relative humidity of 95 ± 5% until testing.

Flowability. The flowability of EGC was measured by the mini-slump test according to Chinese standard GB/T 2419-2005 (Chinese Standard 2005). A 50-mm high truncated core with an upper diameter of 70 mm and a lower diameter of 100 mm was filled with fresh composites and placed on a wet and levelled steel plate. During the test, the mould was lifted up and the table was dropped 25 times in 15 s. The average of the spread diameters in two perpendicular directions was recorded.

Density. The density of the EGC was measured to evaluate its porosity according to ASTM C642 (ASTM 2013). Three cylindric samples with a diameter of 75 mm and a height of 150 mm were utilised for each mix after 28-day curing.

Compression test. The compressive strength of EGC was determined according to BS EN 1015-11 (BS 2019). Three 40 mm cubic specimens were used in the compression test. The compressive load was applied at a rate of 0.6 MPa/s, and 3-day, 7-day and 28-day compressive strengths of EGCs were tested.

Uniaxial tensile test. Four EGC dumbbell specimens were prepared for each mixture in the uniaxial tensile test in accordance with Japan Society of Civil Engineers (JSCE 2008). The dimension and details of the tensile test specimen are shown in **Fig. 3**. An universal testing machine was used to conduct the direct tensile test with a loading rate of 0.5 mm/min (JSCE 2008). During the uniaxial tensile test, a pair of linear variable displacement transducers were attached to both sides of the dumbbell specimen to measure the tensile strain within the 80 mm gauge length as shown in **Fig. 4(a)**. Three specimens were polished with white paint to monitor the crack development, and one specimen was painted by speckle pattern for digital image correlation (DIC) as shown in **Fig. 4(b)**. The DIC technique was employed to analyse the crack distribution and development of the EGCs under uniaxial tension. White and black spray painting were utilised to produce random speckle patterns on the surface of samples with a density and randomness from the previous studies (Huang et al. 2022; Xu et al. 2021). The area with a resolution of 572 × 2394 pixels corresponds to a physical area of 30 × 80 mm^2. A subset size of 100 pixels and a step size of 25 pixels are utilized to illustrate the multiple cracking development. A 24.0-megapixel camera (Nikon D5200) was utilised to monitor the crack development within the 80-mm gauge every 10 s, and each pixel in the obtained image represents 50 μm in the physical scale. The DIC has been proved as an effective method to detect the 2-D strain field, and the testing procedure could refer to Huang *et al.* (2021b). It should be noted that mix "Mortar" was not prepared for the uniaxial tensile test due to its weak tensile strain capacity.

Single fibre pull-out test. Single fibre pull-out test was used to measure the fibre/matrix interfacial bond. A single PE fibre was pulled out from the geopolymer matrix with 2-mm thickness and the test details can be found in the previous study (Curosu et al. 2017). Five specimens were prepared for each mix and the fibre/matrix frictional bond τ can be calculated by Eq. (1) (Lin and Li 1997).

$$\tau = \frac{P}{\pi d_f l_e} \tag{1}$$

where P is the peak load, d_f is the fibre diameter (i.e., 24 μm in this study), and l_e is the fibre embedment length (i.e., 2 mm in this study).

Microstructure analysis. Scanning electron microscope (SEM, ∑IGMA™ field emission scanning electron microscope) analysis was conducted to characterise the fibre status and morphology of the fibre/matrix interface. After the uniaxial tensile test, small pieces of specimens at the region of main crack were collected for the SEM analysis. The small pieces were then immersed in isopropanol for 24h and then dried for 5h at 40°C by an oven to stop the reaction (Kaja et al. 2018).

3 Results and Discussion

3.1 Flowability

Fig. 5 compares the flowability of EGCs with various dosages and lengths of PE fibres. It is readily seen that the incorporation of PE fibres significantly decreases the flowability of EGC. This is mainly attributed to the fact that the randomly distributed fibres, which could form a skeleton in the composites, hinder the free flow of geopolymer mortar. For the EGCs with the same fibre length, increasing the fibre dosage gradually decreases their flowability, particularly for those with longer PE fibres. For instance, increasing the fibre dosage from 1.75% to 2.0% decreases the spread diameter of the EGCs with 12 mm and 18 mm fibres by 3.5% and 13.4%, respectively. This is attributed to the densified network of fibres within EGC with a higher fibre dosage, which increases the yield stress of fresh composites (Ranjbar and Zhang 2020). This is in line with the findings on the PVA fibre reinforced geopolymer composites (Ranjbar and Zhang 2020), in which reported that the incorporation of 0.5% and 1.0% of PVA fibre decreases the flowability of geopolymer composites by around 15% and 40%, respectively. For the EGCs with the same fibre dosage, increasing the fibre length gradually decreases their flowability. The spread diameters of the EGCs with 12 mm and 18 mm fibres are 4.1% and 14.5% lower than that of the EGC with 6 mm fibres, respectively. Similar results are also reported in the previous study (Ranjbar and Zhang 2020), in which reported the use of longer fibres (i.e., with a higher aspect ratio) decreases the flowability of composites due to the increased yield stress (Ranjbar and Zhang 2020; Si et al. 2020) and the reduced homogeneity of the composites (Said and Razak 2015; Pakravan and Ozbakkaloglu 2019). However, further investigation is needed to reveal the effect of PE fibre dosage and length on the yield stress of fresh EGCs. To sum up, the use of higher PE fibre dosage and longer PE fibre decreases the flowability of EGC.

3.2 Density

Fig. 6 shows the density of the EGCs with various fibre dosages and lengths. For the EGCs with different fibre dosages, the incorporation of 1.5% or 1.75% of 12 mm PE fibres results in similar density, while further increasing the fibre dosage to 2.0% slightly decreases the density of EGCs. Besides, the density of 18 mm fibre reinforced EGCs decreases by 1.5% when the fibre dosage increases from 1.5% and 2.0%. This indicates that increasing the fibre dosage causes more pores entrapped inside EGCs, especially for those with 18 mm fibres. In addition, the use of longer fibres decreases the density of EGCs, which indicates that there are more pores entrapped inside EGCs with longer fibres. Therefore, a high fibre dosage or a longer fibre length introduces more voids into the composites and consequently reduces the density of EGCs.

3.3 Compressive strength

Fig. 7 presents the compressive strengths of the EGCs at different ages. Overall, the compressive strengths of EGCs with various fibre dosages and lengths increase with the curing time. The use of PE fibres has a marginal impact on the compressive strength of EGC, particularly for those with short PE fibres (e.g., 6 mm or 12 mm). This is combinedly caused by the positive fibre bridging effect (Nematollahi et al. 2014) and the negative air entrapping effect (Li and Mishra 1992). For the EGCs with the same fibre length, the early compressive strengths increase and then decrease as the fibre dosage increases from 1.5% to 2.0%. For example, the 3-day compressive strength of the EGC with 1.75% of 12 mm fibres is 6.1% and 4.5% higher than that with 1.5% and 2.0% of 12 mm fibres, respectively. The strength reduction for EGCs with excessive fibres (e.g., at a dosage of 2.0%) could be caused by the air entrapping effect as discussed in section **3.2**. The 28-day compressive strengths of EGCs with 12 mm fibres gradually increase with the fibre dosage. For instance, increasing the fibre dosage from 1.5% to 2.0% enhances the 28-day compressive strength of the EGCs with 12 mm PE fibres by 9.0%, which is mainly attributed to the fibre bridging effect.

Differently, increasing the fibre dosage from 1.5% to 2.0% slightly decreases the 28-day compressive strength of EGCs with 18 mm PE fibres by 3.9% due to the air entrapping effect caused by the reduced homogenous of EGC. This can be verified by the reduced flowability and density of EGC with a high dosage of 18 mm PE fibres, which introduces more entrapped pores inside EGC. It can be found that the influence of fibre dosage on the 28-day compressive strength strongly depends on the fibre length. The fibre-bridging effect dominates the compressive strength enhancement for the EGCs with 12 mm fibres, while the air entrapping effect mainly controls the compressive strength reduction for the EGCs with 18 mm fibres. For the EGCs with 2% of PE fibres, increasing the fibre length from 6 mm to 12 mm has a marginal impact on their compressive strengths at various ages. Although the use of longer fibres (i.e., 12 mm) can enhance the fibre bridging effect, the air entrapping effect caused by 2% of fibres tends to be detrimental to its compressive strength. However, further increasing the fibre length to 18 mm significantly decreases the compressive strength of EGCs. For example, the 28-day compressive strength of the EGC with 2% of 18 mm fibres is 12.4% lower than that with 2% of 12 mm fibres. This is because the use of 18 mm fibres significantly reduces the flowability of EGC and subsequently introduces more voids in the matrix.

3.4 Tensile performance

Fig. 8 shows the uniaxial tensile stress-strain curves of the EGCs with various dosages and lengths of PE fibres. Here, the tensile stress-strain curves are plotted based on the tensile force measured by a load cell and the deformation measured by two linear variable displacement transducers. The crack patterns of EGCs at the ultimate tensile strains are also presented in **Fig. 8**. It is readily seen that all the EGCs exhibit the strain-hardening behaviour and multiple-cracking properties. Their tensile strengths and ultimate tensile strains of EGCs vary with the fibre dosage and length as summarised in **Fig. 9**. Here, the tensile strength is determined as the maximum tensile stress, and the ultimate tensile strain is defined as the tensile strain corresponding to 90% of the peak stress in the descending branch (Yu et al. 2019). As seen in **Fig. 9**, the tensile strength of the EGCs with 12 mm PE fibres first increases by 17.6% as the fibre dosage increases from 1.5% to 1.75%, followed by a slight reduction as the fibre dosage further increases to 2.0%. Differently, the tensile strength of the EGC with 1.5% of 18 mm fibres is 12.0% and 3.7% higher than that with 1.75% and 2.0% of 18 mm PE fibres, respectively. The reduction of tensile strength for EGC with a high fibre dosage (e.g. 2.0%) is mainly caused by the fibre cluster (Chen et al. 2021). This also indicates that using excessive fibres may cause the problem of fibre clusters, particularly for EGCs with long PE fibres. For the EGCs with the same fibre dosage, the tensile strength of the EGC with 2% of 18 mm fibres is 42.0% and 13.6%

higher than that of the EGCs incorporating 2% of 6 mm and 12 mm fibres, respectively. It demonstrates that increasing the fibre length gradually increases the tensile strength of EGC, which agrees well with the theoretical design proposed by Li *et al.* (1995).

For the deformation capacity of EGC, a higher fibre dosage slightly improves the ultimate tensile strain of EGCs with the same fibre length. For instance, increasing the fibre dosage from 1.75% to 2.0% enhances the ultimate tensile strain of the EGCs reinforced by 12 mm and 18 mm PE fibres by 2.6% and 6.0%, respectively. Similar findings have also been reported by Huang *et al.* (2021a). For the EGCs with 2% of fibres, increasing the fibre length enhances their tensile strain capacities. Specifically, the EGC with 2% of 18 mm PE fibres achieves the highest ultimate tensile strain of 11.3%, which is 50.9% and 148.0% higher than that of the EGCs reinforced by 12 mm and 6 mm PE fibres, respectively. In general, increasing either fibre dosage or length is an effective way to improve the tensile strain capacity of EGC. Considering the potential fibre cluster in EGCs with excessive fibres or long fibres, it is recommended to adopt 1.5% of 18 mm fibres for EGC to achieve superior tensile performance.

3.5 Crack behaviour

Table 3 summarises the average crack widths in the EGCs at the tensile strain levels of 1.0%, 2.0%, 3.0%, 4.0% and failure. Here, the average crack width is calculated by using the elongation divided by the number of cracks at the various tensile strain levels. It can reflect the full-range crack development of EGCs during the tensile test and is suitable for characterising the multiple cracking behaviour. The linear correlation is applied to fit the relationship between the average crack width and corresponding tensile strain, and their linear relationships and the correlation coefficients are also listed in Table 3. It can be found that the correlation coefficient r is in the range of 0.917-0.999, indicating a strong linear correlation between the average crack width and its corresponding tensile strain.

Fig. 10 compares the linear correlations between the average crack width and its corresponding tensile strain for the EGCs. For the EGCs with the same fibre length, increasing the fibre dosage decreases their average crack widths, particularly at the later loading stage. For instance, the average crack width of the EGCs with 18 mm PE fibres at 9% tensile strain decreases from 250 μm to 161 μm as the fibre dosage increases from 1.5% to 2.0%. This indicates that the crack control ability is improved for EGC with a higher fibre dosage. For the EGCs with the same fibre dosage, increasing the fibre length from 6 mm to 18 mm gradually improves their crack control ability as reflected by the reduced slope of crack width-strain curves, as seen in **Fig. 10**. Therefore, increasing either the fibre dosage or length is able to improve the crack control capacity of EGC.

In addition, digital image correlation (DIC) was mainly utilised to obtain the crack distribution and development in the EGCs. The multiple cracking pattern and strain distributions of the EGC samples at various strain levels of 20%ε_u, 40%ε_u, 60%ε_u, 80%ε_u and 100%ε_u are analysed, where ε_u is the ultimate tensile strain of the EGC specimens. **Fig. 11** compares the tensile strain fields and crack patterns of the EGCs reinforced by 2% of 6 mm, 12 mm, or 18 mm PE fibres. The upper limit of tensile strain is set as 2.5% in the bar legend to clearly present the crack distribution and multiple cracking behaviour. Here, red colour indicates higher local tensile strain, while blue/green colour represents lower local tensile strain. Overall, all the EGCs incorporating 2% of 6 mm, 12 mm and 18 mm PE fibres show obvious multiple cracking behaviour, and the number of cracks increases with the tensile strain. At the failure stage (i.e., the last DIC photo), the EGCs with 2% of 12 mm or 18 mm PE fibres exhibit almost saturated cracks. By contrast, the EGCs with 6 mm fibres exhibit obvious low-strain zones (i.e., blue and green zones), which indicates that 12 mm and 18 mm fibres are more effective for EGC to accomplish excellent saturated multiple cracking behaviour.

3.6 SEM analysis

Fig. 12 presents the SEM images of cross-sections around the main crack in the EGCs containing 2% of 6 mm, 12 mm, and 18 mm PE fibres. In general, the failure mechanisms of fibres during the uniaxial tensile test are different for EGCs with various fibre lengths. There are obvious pores in the EGC with 6 mm PE fibres as annotated in **Fig. 12(a)**, which are resulted from the fibre pull-out process. It demonstrates that the EGC with short fibres (i.e., 6 mm in this study) tends to fail with fibre pull-out. Consequently, the EGC with 6 mm PE fibres exhibits relatively lower tensile strength and strain capacity as compared with the other EGCs. For the EGCs containing 2% of 12 mm or 18 mm PE fibres, the fibre cluster occurs as shown in **Fig. 12(b)** and **12(c)**. This explains that EGC with a higher fibre dosage possibly shows a lower tensile strength due to the reduced effective bonding area. As seen in **Fig. 12(d),** the surfaces of 6 mm fibres pulled out from the matrix are still smooth without obvious change in the diameter. Differently, fibre rupture occurs in the EGCs reinforced by 2% of 12 mm or 18 mm PE fibres, accompanied by the change of fibre diameter as shown in **Fig. 12(e)** and **11(f)**. This indicates a longer fibre reinforcement is more effective in resisting the tensile stress and consequently improves the tensile strength and tensile strain capacity of EGC.

3.7 Prediction of tensile strength

The tensile strengths of the developed PE fibre reinforced EGCs are predicted based on the model proposed by Naaman *et al*. (2008) as shown in Eq. **(2)**.

$$\sigma_{pc} = \lambda \tau V_f \frac{L_f}{d_f} \qquad \textbf{(2)}$$

where σ_{pc} is the tensile strength, λ represents the group effect, spalling effect, fibre orientation and average embedded length during pull out of a large number of inclined fibres. L_f, d_f and V_f are the fibre length, diameter, and dosage, respectively. τ is the fibre/matrix frictional bond. It is noted that only the frictional bond is considered at the interface between PE fibre and matrix (Ranade et al. 2015), and the average frictional bond is measured as 0.72 (±0.21) MPa in this study. **Fig. 13(a)** presents a relatively strong quadratic correlation between tensile strength and V_fL_f/d_f. Similar results are also found in the previous study (Wille et al. 2014), in which a strong dependency between tensile strength and fibre volume is correlated by $\sigma_{pc}=-0.9V_f^2+9V_f$. Besides, the tensile strength is the product of λ, fibre/matrix frictional bond τ, fibre dosage V_f, and fibre aspect ratio L_f/d_f according to the prediction model proposed by Naaman (Eq. (2)). Among them, the fibre/matrix frictional bond τ can be regarded as a constant for a given matrix and type of fibre. Considering the fibre aspect ratio is not related to the fibre dosage, it can be inferred that the λ is linearly correlated with V_f to satisfy the correlation between tensile strength and V_f^2. Furthermore, λ relating to the group effect, fibre orientation and average embedded length is influenced by the fibre length and diameter. Therefore, it can be inferred that the λ is linearly correlated with $V_f L_f/d_f$. In this study, the value of λ is determined based on a linear regression using the test results (λ=-0.0761 V_fL_f/d_f+1.7985). As seen in **Fig. 13(b),** the value of λ gradually reduces with the V_fL_f/d_f, illustrating the increase of V_fL_f/d_f decreases the efficiency of tensile strength improvement. This relationship between λ and V_fL_f/d_f is subsequently applied to calculate the λ and tensile strength of EGC based on **Eq. (2)**. **Table 4** shows the comparison between measured and predicted tensile strengths of EGCs in the different studies. It can be found that **Eq. (2)** with the proposed parameters slightly underestimates the tensile strength of EGC in most cases, which is conservative and safe for the design of EGC. This is related to the underestimation of parameter λ as it cannot reflect the influence of fibre cluster, particularly for the EGC with a high dosage of long fibres. Overall, it shows that the ratio of measured to predicted tensile strength of EGC is 1.03, indicating that the tensile strength of PE fibre reinforced EGCs cured at ambient temperature can be accurately predicted based on the fibre/matrix frictional bond, fibre dosage, length, and diameter.

4 Environmental Impacts Assessment

To evaluate the sustainability aspect of the developed EGCs, material sustainability indicators (MSIs) based on the materials and energy flow in the manufacturing process (i.e. cradle-to-gate) were adopted (Yang et al. 2007). In this study, CO_2 emission and embodied energy were used as the MSIs. The MSIs of raw materials collected from the literature and environmental reports were summarised in **Table 5**. It is noted the embodied energy and carbon emission of sodium silicate can be referred to the previous study (Fawer et al. 1999) as their chemical composites of sodium silicate are similar in both studies. In addition, the conventional M45 ECC (Yang et al. 2007) and HTS-ECC (Yu and Leung 2020) were included for comparison. **Table 6** shows the mix proportions and tensile performance of HTS-ECC, M45 ECC, and EGC. The EGC incorporating 2% of PE fibres was selected for comparison as it has the highest embodied energy and carbon emission.

Fig. 14 compares the unit-volume embodied energy and carbon of HTS-ECC, conventional M45 ECC and EGC with 2% of PE fibres. Overall, the EGC reinforced by 2% of PE fibres in this study shows lower unit-volume embodied energy and carbon than the HTS-ECC and conventional M45 ECC. The unit-volume embodied energy of the EGC incorporating 2% of PE fibres is 55% and 22% lower than that of HTS-ECC and conventional M45 ECC, respectively. The unit-volume embodied carbon of the EGC reinforced by 2% of PE fibres is 80% and 53% less than that of HTSECC and conventional M45 ECC, respectively. This is mainly due to the use of geopolymer synthesised from the industrial by-products (i.e., fly ash and GGBS) as the replacement of cement. By contrast, a large amount of cement and superplasticiser used in HTS-ECC dramatically increases the unit-volume embodied energy and carbon of composites. This finding coincides with several previous studies which demonstrated that the use of geopolymer binder as an alternative to cement can offer advantages in the environmental impacts of fibre-reinforced composites (Ohno and Li 2018; Nematollahi et al. 2017a). Apart from the PE fibres, the energy consumption and carbon emission in EGC are mainly caused by using the alkali activator. Compared to the EGC incorporating 2% of PE fibres, the EGC with 1.5% of 18 mm PE fibres attains further improved environmental impact due to the use of reduced fibre dosage.

5 Conclusions

This paper developed a high-tensile-strength and high-tensile-strain capacity PE fibre reinforced EGC cured at ambient temperature. The influences of fibre dosage and length on the flowability, compressive strength, tensile performance, and crack control ability of EGC were investigated. Based on the experimental results and discussion, the following conclusions could be drawn:

1) The incorporation of PE fibres significantly reduces the flowability of EGC due to the formed skeleton by fibres. Increasing either fibre dosage or length reduces the homogeneity of EGC, and then gradually decreases its flowability.

2) Increasing the fibre dosage from 1.5% to 2.0% enhances the fibre bridge effect in EGCs with 12 mm fibres, which enhances their compressive and tensile strengths by 9.0% and 12.7%, respectively.

However, increasing the dosage of 18 mm fibres from 1.5% to 2.0% introduces more air voids to EGCs and subsequently decreases their compressive and tensile strengths by 3.8% and 3.6%, respectively. In addition, excessive fibres tend to cause fibre cluster, which decreases the tensile strength of EGC. Increasing the fibre dosage can enhance the crack control ability and tensile strain capacity of EGC.

3) The use of 18 mm fibres is detrimental to the compressive strength of EGC due to the magnified air entrapping effect. However, increasing the fibre length from 6 mm to 18 mm can improve the tensile strength, crack control ability, and deformability of EGC due to the enhanced fibre bridging effect. Besides, using 2% of 12 mm or 18 mm PE fibres is beneficial to the accomplishment of saturated multiple cracking behaviour.
4) The tensile strength of PE fibre reinforced EGC can be accurately predicted by a modified model with the considerations of the fibre/matrix frictional bond, fibre dosage, length, and diameter. However, the modified prediction model slightly underestimates the tensile strength of EGC due to the omission of fibre cluster effect, particularly for the EGC with a high dosage of long fibres.
5) The developed EGCs with PE fibres show improved environmental benefits compared to the conventional ECC in terms of embodied energy and carbon. This demonstrates that ambient temperature cured EGC with PE fibres could be a sustainable alternative to conventional ECC without compromising the high tensile strength but improving the deformability.

Data availability

Some or all data, models, or code that support the findings of this study are available from the corresponding author upon reasonable request.

Acknowledgement

The authors wish to acknowledge the financial support from the Ningbo Science and Technology Bureau under Commonweal Programme (Nos.: 2022S177 and 2021S097) and Zhejiang Commonweal Programme (No.: LGF22B060009). The Zhejiang Provincial Department of Science and Technology is acknowledged for this research under its Provincial Key Laboratory Programme (No.: 2020E10018).

References

Alrefaei, Y., and J. G. Dai. 2018. "Tensile behavior and microstructure of hybrid fiber ambient cured one-part engineered geopolymer composites." *Constr. Build. Mater.*, 184: 419–431. https://doi.org/10.1016/j.conbuildmat.2018.07.012.

ASTM. 2013. *Standard test method for density, absorption, and voids in hardened concrete.* ASTM C642. West Conshohocken, PA: ASTM.

Chinese Standard. 2005. *Test Method for Fluidity of Cement Mortar*, GB/T 2419-2005. Beijing: China Architecture & Building Press.

BS (British Standard). 2019. *Methods of test for mortar for masonry. Part 11: Determination of flexural and compressive strength of hardened mortar.* EN 1015-11. Brussels, Belgium: BS.

Chen, W., Y. Xie, B. Li, B. Li, J. Wang, and N. Thom. 2021. "Role of aggregate and fibre in strength and drying shrinkage of alkali-activated slag mortar." *Constr. Build. Mater.*, 299: 124002. https://doi.org/10.1016/j.conbuildmat.2021.124002.

Choi, J. Il, B. Y. Lee, R. Ranade, V. C. Li, and Y. Lee. 2016a. "Ultra-high-ductile behavior of a polyethylene fiber-reinforced alkali-activated slag-based composite." *Cem. Concr. Compos.*, 70: 153–158. https://doi.org/10.1016/j.cemconcomp.2016.04.002.

Choi, J. Il, K. Il Song, J. K. Song, and B. Y. Lee. 2016b. "Composite properties of high-strength polyethylene fiber-reinforced cement and cementless composites." *Compos. Struct.*, 138: 116–121. https://doi.org/10.1016/j.compstruct.2015.11.046.

Choi, W. C., H. Do Yun, J. W. Kang, and S. W. Kim. 2012. "Development of recycled strain-hardening cement-based composite (SHCC) for sustainable infrastructures." *Compos. Part B Eng.*, 43 (2): 627–635. https://doi.org/10.1016/j.compositesb.2011.11.060.

Curosu, I., M. Liebscher, V. Mechtcherine, C. Bellmann, and S. Michel. 2017. "Tensile behavior of high-strength strain-hardening cement-based composites (HS-SHCC) made with highperformance polyethylene, aramid and PBO fibers." *Cem. Concr. Res.*, 98 (April): 71–81. https://doi.org/10.1016/j.cemconres.2017.04.004.

Damtoft, J. S., J. Lukasik, D. Herfort, D. Sorrentino, and E. M. Gartner. 2008. "Sustainable development and climate change initiatives." *Cem. Concr. Res.*, 38 (2): 115–127. https://doi.org/10.1016/j.cemconres.2007.09.008.

EFCA. 2002. *EFCA Environmental declaration-superplasticizing admixtures. Superplasticizing Admixtures.* European Federation of Concrete Admixture.

Euro Chlor. 2013. *An Eco-profile and Environmental Product Declaration of the European Chlor-Alkali Industry*.

Farooq, M., A. Bhutta, and N. Banthia. 2020. "Strain-hardening ambient-cured eco-friendly ductile geopolymer composites." *ACI Mater. J.*, 117 (3): 181–189. https://doi.org/10.14359/51724597.

Fawer, M., M. Concannon, and W. Rieber. 1999. "Life cycle inventories for the production of sodium silicates." *Int. J. Life Cycle Assess.*, 4 (4): 207–212. https://doi.org/10.1007/BF02979498.

Frazão, R., and D. C. Peneda. 2004. *Comparative Analysis of the Life Cycle of AT Fibre-cement and NT Fibre-cement*. International Chrysotile Association.

Hammond, G. P., and Jones, C. I. 2008. *Inventory of carbon and energy.* Version 1.6a Univ. Bath. UK

He, S., J. Qiu, J. Li, and E.-H. Yang. 2017. "Strain hardening ultra-high performance concrete (SHUHPC) incorporating CNF-coated polyethylene fibers." *Cem. Concr. Res.*, 98 (January): 50–60. https://doi.org/10.1016/j.cemconres.2017.04.003.

Huang, B.-T., Q.-H. Li, S.-L. Xu, and L. Zhang. 2019. “Static and fatigue performance of reinforced concrete beam strengthened with strain-hardening fiber-reinforced cementitious composite.” *Eng. Struct.*, 199: 109576. https://doi.org/10.1016/j.engstruct.2019.109576.

Huang, B.-T. T., J.-Q. Q. Wu, J. Yu, J.-G. G. Dai, and C. K. Leung. 2020. “High-strength seawater sea-sand Engineered Cementitious Composites (SS-ECC): Mechanical performance and probabilistic modeling.” *Cem. Concr. Compos.*, 114: 103740. https://doi.org/10.1016/j.cemconcomp.2020.103740.

Huang, B. T., Y. T. Wang, J. Q. Wu, J. Yu, J. G. Dai, and C. K. Y. Leung. 2021a. “Effect of fiber content on mechanical performance and cracking characteristics of ultra-high-performance seawater sea-sand concrete (UHP-SSC).” *Adv. Struct. Eng.*, 24 (6): 1182–1195. https://doi.org/10.1177/1369433220972452.

Huang, B. T., K. F. Weng, J. X. Zhu, Y. Xiang, J. G. Dai, and V. C. Li. 2021b. “Engineered/strainhardening cementitious composites (ECC/SHCC) with an ultra-high compressive strength over 210 MPa.” *Compos. Commun.*, 26: 100775. https://doi.org/10.1016/j.coco.2021.100775.

Huang, B. T., J. Q. Wu, J. Yu, J. G. Dai, C. K. Y. Leung, and V. C. Li. 2021c. “Seawater sea-sand engineered/strain-hardening cementitious composites (ECC/SHCC): Assessment and modeling of crack characteristics.” *Cem. Concr. Res.*, 140: 106292. https://doi.org/10.1016/j.cemconres.2020.106292.

Huang, B. T., J. X. Zhu, K. F. Weng, V. C. Li, and J. G. Dai. 2022. “Ultra-high-strength engineered/strain-hardening cementitious composites (ECC/SHCC): Material design and effect of fiber hybridization.” *Cem. Concr. Compos.*, 129. https://doi.org/10.1016/j.cemconcomp.2022.104464.

Huang, X., R. Ranade, and V. C. Li. 2013. “Feasibility Study of Developing Green ECC Using Iron Ore Tailings Powder as Cement Replacement.” *J. Mater. Civ. Eng.*, 25 (7): 923–931. https://doi.org/10.1061/(asce)mt.1943-5533.0000674.

Japan Society of Civil Engineers. 2008. “Recommendations for Design and Construction of High Performance Fiber Reinforced Cement Composites with Multiple Fine Cracks (HPFRCC).” *Concr. Eng. Ser.*, 82: Testing Method 6-10.

Kaja, A. M., A. Lazaro, and Q. L. Yu. 2018. “Effects of Portland cement on activation mechanism of class F fly ash geopolymer cured under ambient conditions.” *Constr. Build. Mater.*, 189: 1113–1123. https://doi.org/10.1016/j.conbuildmat.2018.09.065.

Kan, L., and F. Wang. 2021. “Mechanical properties of high ductile alkali-activated fiber reinforced composites incorporating red mud under different curing conditions.” *Ceram. Int.*, 48 (2): 1999–2011. https://doi.org/10.1016/j.ceramint.2021.09.285.

Kan, L., F. Wang, Z. Zhang, W. Kabala, and Y. Zhao. 2021. “Mechanical properties of high ductile alkali-activated fiber reinforced composites with different curing ages.” *Constr. Build. Mater.*, 306. https://doi.org/10.1016/j.conbuildmat.2021.124833.

Keoleian, G. A., A. Kendall, J. E. Dettling, V. M. Smith, R. F. Chandler, M. D. Lepech, and V. C. Li. 2005. “Life Cycle Modeling of Concrete Bridge Design: Comparison of Engineered Cementitious Composite Link Slabs and Conventional Steel Expansion Joints.” *J. Infrastruct. Syst.*, 11 (1): 51–60. https://doi.org/10.1061/(asce)1076-0342(2005)11:1(51).

Kumar, S., C. Sekhar Das, J. Lao, Y. Alrefaei, and J. G. Dai. 2022. “Effect of sand content on bond performance of engineered geopolymer composites (EGC) repair material.” *Constr. Build. Mater.*, 328: 127080. https://doi.org/10.1016/j.conbuildmat.2022.127080.

Li, V. C. 2019. *Engineered Cementitious Composites (ECC): Bendable Concrete for Sustainable and Resilient Infrastructure.* Springer, Berlin, Heidelberg.

Li, V. C., and C. K. Y. Leung. 1992. “Steady-state and multiple cracking of short random fiber composites.” *J. Eng. Mech.*, 118 (11): 2246–2264.

Li, V. C., D. K. Mishra, and H. C. Wu. 1995. “Matrix design for pseudo-strain-hardening fibre reinforced cementitious composites.” *Mater. Struct.*, 28 (10): 586–595. https://doi.org/10.1007/BF02473191.

Li, V., and D. K. Mishra. 1992. “Micromechanics of fiber effect on the uniaxial compressive strength of cementious composites.” *Fourth Int. Symp. Fibre Reinf. Cem. Concr.*, 400–414.

Lin, Z., and V. C. Li. 1997. “Crack bridging in fiber reinforced cementitious composites with sliphardening interfaces.” *J. Mech. Phys. Solids*, 45 (5): 763–787. article. Elsevier Ltd. https://doi.org/10.1016/S0022-5096(96)00095-6.

Liu, X., G. Lai, J. Guan, S. Qian, Z. Wang, S. Cui, F. Gao, Y. Jiao, and R. Tao. 2021. “Technical optimization and life cycle assessment of environment-friendly superplasticizer for concrete engineering.” *Chemosphere*, 281: 130955. https://doi.org/10.1016/j.chemosphere.2021.130955.

Lương, Q. H., H. H. Nguyễn, J. Il Choi, H. K. Kim, and B. Y. Lee. 2021. “Effects of crumb rubber particles on mechanical properties and sustainability of ultra-high-ductile slag-based composites.” *Constr. Build. Mater.*, 272. https://doi.org/10.1016/j.conbuildmat.2020.121959.

Lyu, B.-C., C. Ding, L.-P. Guo, B. Chen, and A. Wang. 2021. “Basic performances and potential research problems of strain hardening geopolymer composites: A critical review.” *Constr. Build. Mater.*, 287: 123030. https://doi.org/10.1016/j.conbuildmat.2021.123030.

Naaman, A. E. 2008. “High performance fiber reinforced cement composites.” *High-Performance Constr. Mater. Sci. Appl.*, 91-153. Singapore: World Scientific Publishing.

Nath, P., P. K. Sarker, and V. B. Rangan. 2015. “Early age properties of low-calcium fly ash geopolymer concrete suitable for ambient curing.” *Procedia Eng.*, 601–607. https://doi.org/10.1016/j.proeng.2015.11.077

Nematollahi, B., R. Ranade, J. Sanjayan, and S. Ramakrishnan. 2017a. “Thermal and mechanical properties of sustainable lightweight strain hardening geopolymer composites.” *Arch. Civ. Mech. Eng.*, 17 (1): 55–64. https://doi.org/10.1016/j.acme.2016.08.002.

Nematollahi, B., J. Sanjayan, J. Qiu, and E. H. Yang. 2017b. “High ductile behavior of a polyethylene fiber-reinforced one-part geopolymer composite: A micromechanics-based investigation.” *Arch. Civ. Mech. Eng.*, 17 (3): 555–563. https://doi.org/10.1016/j.acme.2016.12.005.

Nematollahi, B., J. Sanjayan, and F. U. A. Shaikh. 2014. “Comparative deflection hardening behavior of short fiber reinforced geopolymer composites.” *Constr. Build. Mater.*, 70: 54–64. https://doi.org/10.1016/j.conbuildmat.2014.07.085.

Ohno, M., and V. C. Li. 2018. “An integrated design method of Engineered Geopolymer Composite.” *Cem. Concr. Compos.*, 88: 73–85. Elsevier Ltd. https://doi.org/10.1016/j.cemconcomp.2018.02.001.

Pakravan, H. R., and T. Ozbakkaloglu. 2019. “Synthetic fibers for cementitious composites: A critical and in-depth review of recent advances.” *Constr. Build. Mater. https://doi.org/10.1016/j.conbuildmat.2019.02.078*

Rafeet, A., R. Vinai, M. Soutsos, and W. Sha. 2019. “Effects of slag substitution on physical and mechanical properties of fly ash-based alkali activated binders (AABs).” *Cem. Concr. Res.*, 122: 118–135. https://doi.org/10.1016/j.cemconres.2019.05.003.

Ranade, R., V. C. Li, and W. F. Heard. 2015. “Tensile rate effects in high strength-high ductility concrete.” *Cem. Concr. Res.*, 68: 94–104. https://doi.org/10.1016/j.cemconres.2014.11.005.

Ranjbar, N., and M. Zhang. 2020. “Fiber-reinforced geopolymer composites: A review.” *Cem. Concr. Compos.*, 107: 103498. https://doi.org/10.1016/j.cemconcomp.2019.103498.

Rovnaník, P. 2010. “Effect of curing temperature on the development of hard structure of metakaolin-based geopolymer.” *Constr. Build. Mater.*, 24 (7): 1176–1183.

https://doi.org/10.1016/j.conbuildmat.2009.12.023.

Said, S. H., and H. A. Razak. 2015. “The effect of synthetic polyethylene fiber on the strain hardening behavior of engineered cementitious composite (ECC).” *Mater. Des.*, 86: 447–457. Elsevier Ltd. https://doi.org/10.1016/j.matdes.2015.07.125.

Shaikh, F. U. A., A. Fairchild, and R. Zammar. 2018. “Comparative strain and deflection hardening behaviour of polyethylene fibre reinforced ambient air and heat cured geopolymer composites.” *Constr. Build. Mater.*, 163: 890–900. https://doi.org/10.1016/j.conbuildmat.2017.12.175.

Si, W., M. Cao, and L. Li. 2020. “Establishment of fiber factor for rheological and mechanical performance of polyvinyl alcohol (PVA) fiber reinforced mortar.” *Constr. Build. Mater.*, 265. https://doi.org/10.1016/j.conbuildmat.2020.120347.

Wang, Y., H. Zhong, and M. Zhang. 2022. “Experimental study on static and dynamic properties of fly ash-slag based strain hardening geopolymer composites.” *Cem. Concr. Compos.*, 129. https://doi.org/10.1016/j.cemconcomp.2022.104481.

Wei, J., C. Wu, Y. Chen, and C. K. Y. Leung. 2020. “Shear strengthening of reinforced concrete beams with high strength strain-hardening cementitious composites (HS-SHCC).” *Mater. Struct.*, 53 (4): 102. https://doi.org/10.1617/s11527-020-01537-1.

Wille, K., S. El-Tawil, and A. E. Naaman. 2014. “Properties of strain hardening ultra high performance fiber reinforced concrete (UHP-FRC) under direct tensile loading.” *Cem. Concr. Compos.*, 48: 53–66. https://doi.org/10.1016/j.cemconcomp.2013.12.015.

Wu, H.-C., and V. C. Li. 1999. “Fiber/cement interface tailoring with plasma treatment.” *Cem. Concr. Compos.*, 21 (3): 205–212. https://doi.org/10.1016/S0958-9465(98)00053-5.

Wu, H., J. Yu, Y. Du, and V. C. Li. 2021. “Mechanical performance of MgO-doped Engineered Cementitious Composites (ECC).” *Cem. Concr. Compos.*, 115. https://doi.org/10.1016/j.cemconcomp.2020.103857.

Xu, L. Y., B. T. Huang, and J. G. Dai. 2021. “Development of engineered cementitious composites

(ECC) using artificial fine aggregates." *Constr. Build. Mater.*, 305. https://doi.org/10.1016/j.conbuildmat.2021.124742.

Yang, E. H., Y. Yang, and V. C. Li. 2007. "Use of high volumes of fly ash to improve ECC mechanical properties and material greenness." *ACI Mater. J.*, 104 (6): 620–628.

Yang, Z., M. Yu, Y. Liu, X. Chen, and Y. Zhao. 2019. "Synthesis and performance of an environmentally friendly polycarboxylate superplasticizer based on modified poly(aspartic acid)." *Constr. Build. Mater.*, 202: 154–161. https://doi.org/10.1016/j.conbuildmat.2018.12.148.

Yu, J., and C. K. Y. Leung. 2020. *Using Limestone Calcined Clay to Improve Tensile Performance and Greenness of High-Tensile Strength Strain-Hardening Cementitious Composites (SHCC)*. *RILEM Bookseries*. Springer Singapore.

Yu, J., C. K. Y. Leung, and V. C. Li. 2019. "Why nominal cracking strength can be lower for later cracks in strain-hardening cementitious composites with multiple cracking?" *10th Int. Conf. Fract. Mech. Concr. Concr. Struct.*, G. Pijaudier-Cabot, P. Grassl, and C. La Borderie, eds., 1–9. Bayonne, France.

Yu, K.-Q., J.-G. Dai, Z.-D. Lu, and C.-S. Poon. 2018. "Rate-dependent tensile properties of ultra-high performance engineered cementitious composites (UHP-ECC)." *Cem. Concr. Compos.*, 93 (June): 218–234. Elsevier. https://doi.org/10.1016/j.cemconcomp.2018.07.016.

Zhang, D., J. Yu, H. Wu, B. Jaworska, B. R. Ellis, and V. C. Li. 2020. "Discontinuous micro-fibers as intrinsic reinforcement for ductile Engineered Cementitious Composites (ECC)." *Compos. Part B Eng.*, 184: 107741. https://doi.org/10.1016/j.compositesb.2020.107741.

Zhong, H., and M. Zhang. 2021. “Effect of recycled tyre polymer fibre on engineering properties of sustainable strain hardening geopolymer composites.” *Cem. Concr. Compos.*, 122. https://doi.org/10.1016/j.cemconcomp.2021.104167.

List of Figures

Table 1. Chemical compositions of Fly Ash and GGBS.

Materials	Al_2O_3 (%)	SiO_2 (%)	CaO (%)	Fe_2O_3 (%)	MgO (%)	SO_3 (%)	TiO_2 (%)	K_2O (%)
Fly Ash	36.22	48.56	4.13	5.84	0.31	0.19	1.80	1.03
GGBS	13.97	29.02	43.52	0.37	8.97	0.42	2.13	0.51

Table 2. Mix proportions of the EGCs reinforced by PE fibres in mass.

Mix ID	Binder		Alkali Dosage	Silicate Modulus	Water/ Binder	Sand/ Binder	Fibre Length (mm)	PE Fibres (vol.%)
	Fly ash	GGBS						
Mortar	0.5	0.5	4.5%	2.25	0.33	0.30	/	/
PE6-2%	0.5	0.5	4.5%	2.25	0.33	0.30	6	2.00
PE12-1.5%	0.5	0.5	4.5%	2.25	0.33	0.30	12	1.50
PE12-1.75%	0.5	0.5	4.5%	2.25	0.33	0.30	12	1.75
PE12-2.0%	0.5	0.5	4.5%	2.25	0.33	0.30	12	2.00
PE18-1.5%	0.5	0.5	4.5%	2.25	0.33	0.30	18	1.50
PE18-1.75%	0.5	0.5	4.5%	2.25	0.33	0.30	18	1.75
PE18-2.0%	0.5	0.5	4.5%	2.25	0.33	0.30	18	2.00

Table 3. Tensile strain level versus corresponding average crack width for the EGCs with PE fibres.

Mix	Tensile strain, *ε* (%) & Average crack width, *w* (μm)						Linear relationship	Correlation coefficient, *r*
6mm-2.0%	*ε*	1.0	2.0	3.0	4.0	4.2	$\varepsilon = 17.6\, w + 38.9$	0.999
	w	57.1	72.7	92.3	110.3	111.5		
12mm-1.5%	*ε*	1.0	2.0	3.0	4.0	6.5	$\varepsilon = 22.5\, w + 85.9$	0.988
	w	114.3	123.1	160.0	168.4	234.5		
12mm-1.75%	*ε*	1.0	2.0	3.0	4.0	8.26	$\varepsilon = 17.7\, w + 40.5$	0.964
	w	61.5	76.2	92.3	106.7	188.8		
12mm-2.0%	*ε*	1.0	2.0	3.0	4.0	7.9	$\varepsilon = 14.2\, w + 49.8$	0.997
	w	61.5	80.0	96.0	103.2	161.0		
18mm-1.5%	*ε*	1.0	2.0	3.0	4.0	10.5	$\varepsilon = 11.9\, w + 142.5$	0.970
	w	160.0	177.8	160.0	188.2	271.0		
18mm-1.75%	*ε*	1.0	2.0	3.0	4.0	9.8	$\varepsilon = 6.2\, w + 160.9$	0.917
	w	160.0	177.8	171.4	200.0	218.4		
18mm-2.0%	*ε*	1.0	2.0	3.0	4.0	11.0	$\varepsilon = 7.8\, w + 91.0$	0.963
	w	100.0	94.1	126.3	123.1	175.5		

Table 4. Comparison of measured and predicted tensile strengths by **Eq. (2).**

Ref.	V_fL_f/d_f	Measured σ_{pc} (MPa)	Predicted λ	τ (MPa)	Predicted σ_{pc} (MPa)	Ratio of measured to predicted σ_{pc}
This study	5	5.48	1.42	0.72	5.11	1.07
	7.5	6.08	1.23	0.72	6.64	0.92
	8.75	7.15	1.13	0.72	7.14	1.00
	10	6.85	1.04	0.72	7.48	0.92
	11.25	8.07	0.94	0.72	7.65	1.05
	13.125	7.21	0.80	0.72	7.57	0.95
	15	7.78	0.66	0.72	7.11	1.09
Kan and Wang (2021)	9.5	4.79	1.08	0.42	4.30	1.11
	9.5	4.88	1.08	0.43	4.40	1.11
Kan et al. (2021)	10	2.92	1.04	0.27	2.81	1.04
	10	3.55	1.04	0.35	3.64	0.98
	10	5.05	1.04	0.48	4.99	1.01
	10	5.77	1.04	0.51	5.30	1.09
	10	5.99	1.04	0.57	5.92	1.01

Table

10	5.91	1.04	0.55	5.71	1.04
				Average	1.03

5. Cradle-to-gate embodied carbon and embodied energy of raw materials

Material	Embodied Energy (MJ/kg)	Embodied Carbon (kg eq. CO_2/kg)
Type I Portland Cement	5.5 (Hammond and Jones 2008)	0.912 (Hammond and Jones 2008)
Fly Ash	0.1 (Hammond and Jones 2008)	0.008 (Hammond and Jones 2008)
GGBS	1.6 (Hammond and Jones 2008)	0.083 (Hammond and Jones 2008)
Sodium Hydroxide Pellets	18 (Euro Chlor 2013)	0.86 (Euro Chlor 2013)
Sodium Silicate (3.3 WR[a], 37% solids)	4.6 (Fawer et al. 1999)	0.43 (Fawer et al. 1999)
Fine Silica Sand	0.067 (Keoleian et al. 2005)	0.023 (Choi et al. 2012)
PCE Superplasticiser (Powder)[b]	42.67 (EFCA 2002)	1.84 (EFCA 2002)
Superplasticiser[c]	36.76 (Huang et al. 2013)	1.48 (Huang et al. 2013)
Chinese Polyethylene Fibre	83.1 (Hammond and Jones 2008)	2.54 (Hammond and Jones 2008)
PVA fibre	101 (Frazão and Peneda 2004)	3.4 (Frazão and Peneda 2004)
Water	0.1 (Hammond and Jones 2008)	0.001 (Hammond and Jones 2008)

Note: [a]: SiO_2-to-Na_2O ratio in sodium silicate (in mass); [b]: Superplasticiser used in HTS-ECC, [c]: Superplasticiser used

Table

in M45

6. Mix proportions and tensile properties of HTS-ECC, conventional ECC M45 and the EGC with 2% of PE fibres in this study.

Material	**Mix proportion (kg/m^3)**									**Tensile strength (MPa)**	**Tensile Strain**
	OPC	**FA**	**GGBS**	**Sand**	**NaOH**	**Na_2SiO_3**	**Water**	**SP [a]**	**Fibre**		
HTS-ECC (Yu and Leung 2020)	1551.4	-	-	465.4	-	-	310.3	10.0	19.4 [b]	8.5	6.4%
ECC M45 (Yang et al. 2007)	571.0	685.0	-	456.0	-	-	332.0	6.8	26.0 [c]	5.9	2.7%
EGC-2% PE	-	547.3	547.3	328.4	20.6	399.7	102.0	-	19.4 [b]	7.8	11.3%

Note: [a] superplasticiser; [b] PE fibre; [c] PVA fibre.

Figure 1

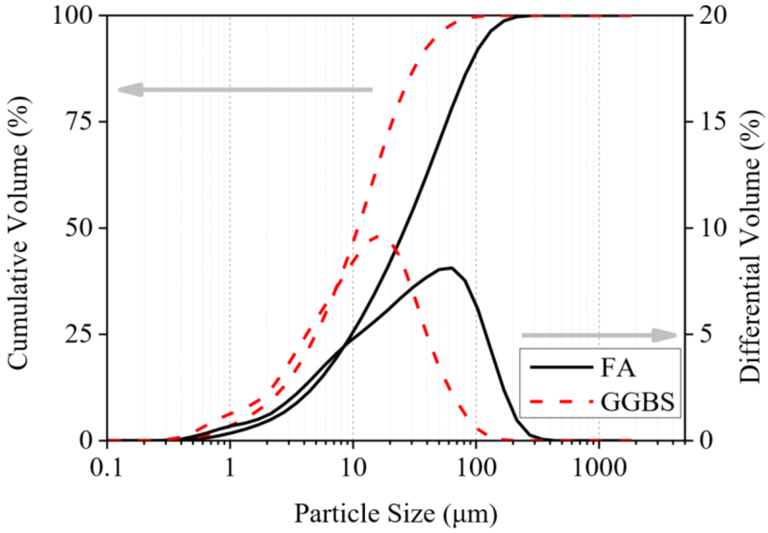

Fig. 1. Particle size distributions of fly ash and GGBS.

Figure 2

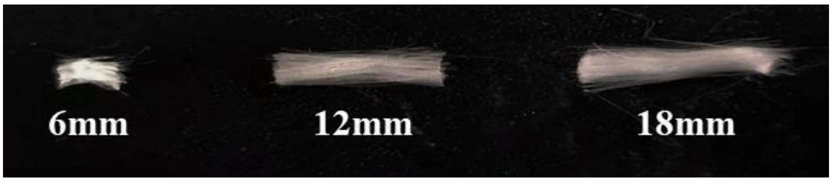

Fig. 2. Photograph of PE fibres with different lengths.

Figure 3

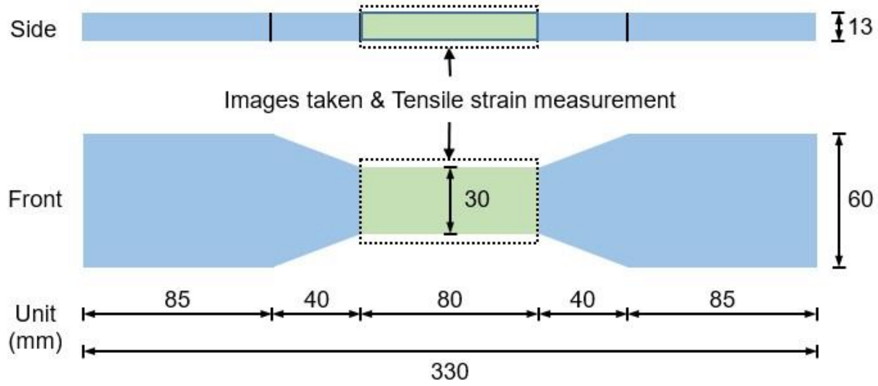

Fig. 3. Dimensions of dumbbell specimen for uniaxial tensile test.

Figure 4

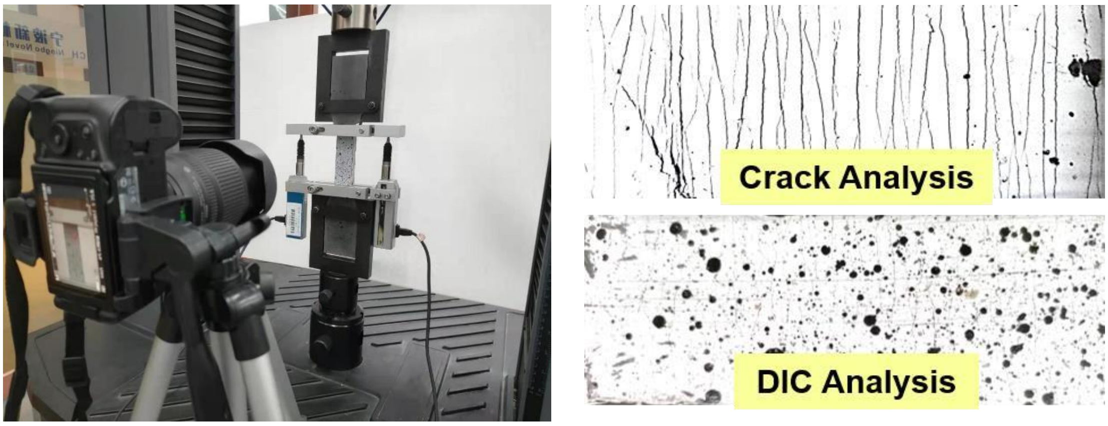

(a) (b)

Fig. 4. (a) Setup of uniaxial tensile test and (b) Paintings for crack and DIC analyses.

Figure 5

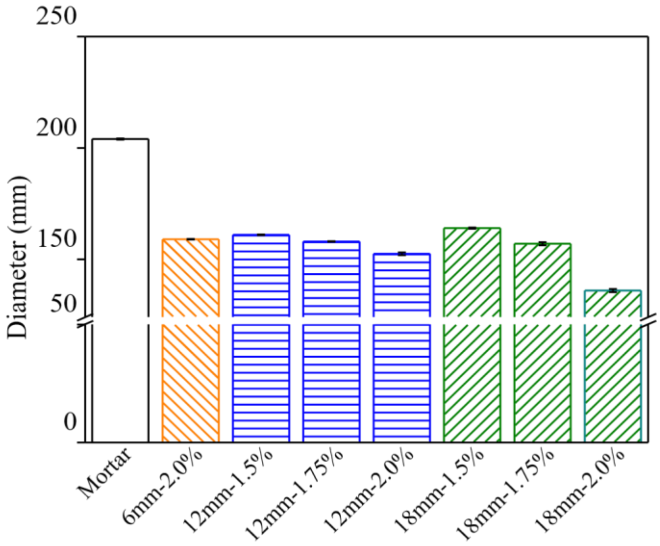

Fig. 5. Flowability of the fresh EGCs with various PE fibre dosages and lengths.

Figure 6

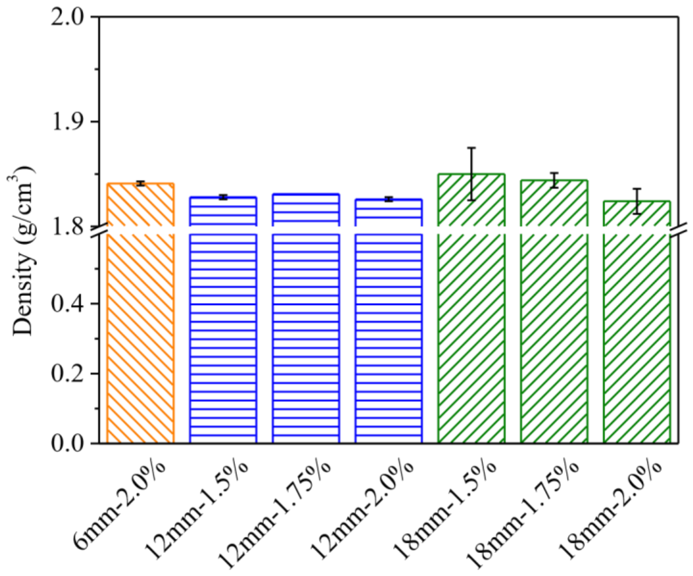

Fig. 6. Density of the EGCs with various PE fibre dosages and lengths.

Figure 7

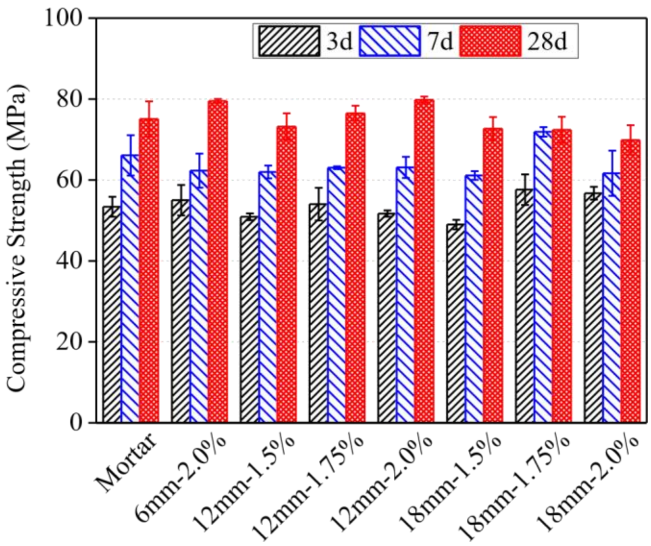

Fig. 7. Compressive strength of the EGCs with various PE fibre dosages and lengths.

Figure 8

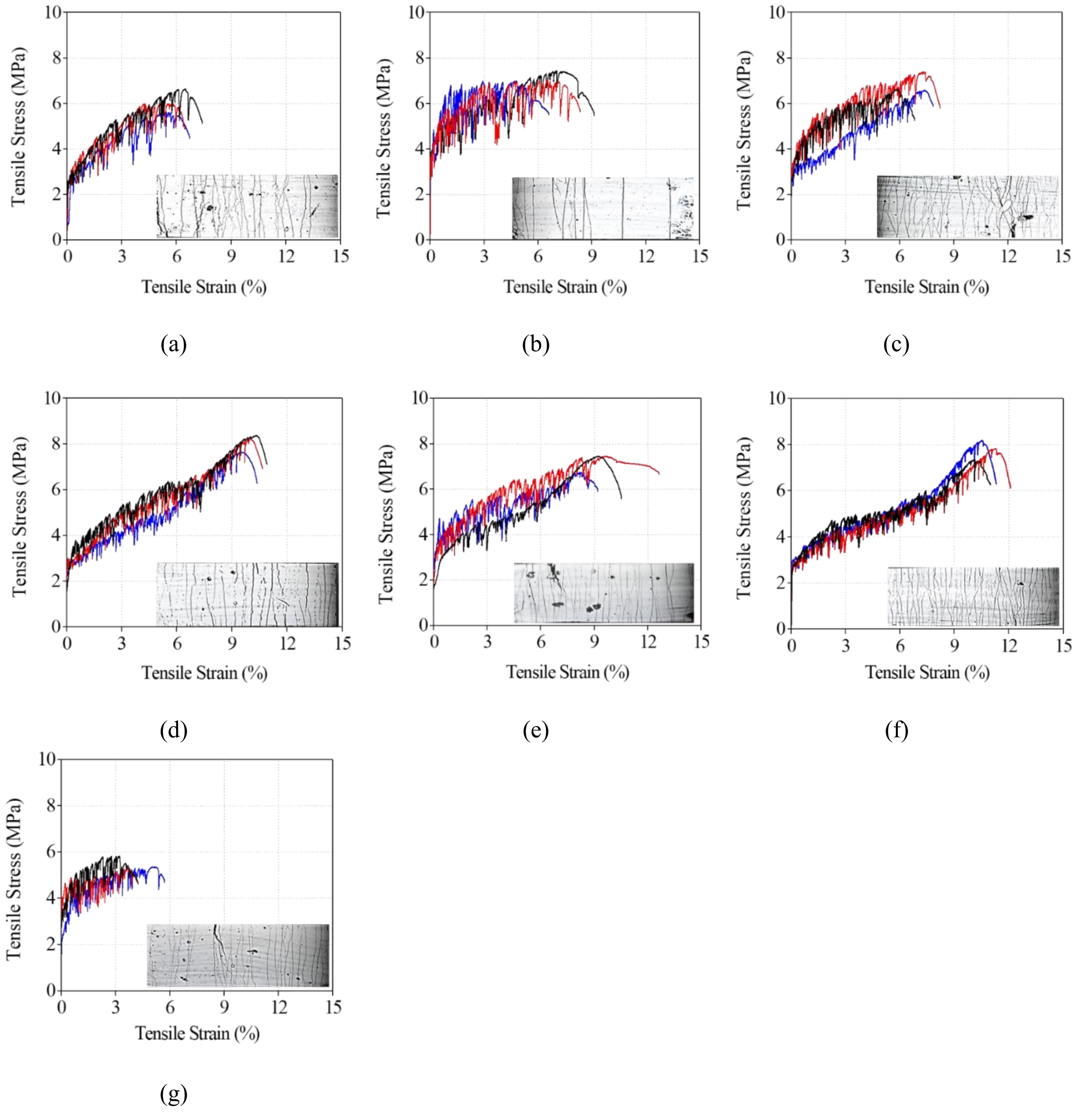

Fig. 8. Tensile stress-strain curves of the EGCs with PE fibres: (a) PE12-1.5%, (b) PE12-1.75%, (c) PE12-2.0%, (d) PE18-1.5%, (e) PE18-1.75%, (f) PE18-2.0%, and (g) PE6-2.0%.

Figure 9

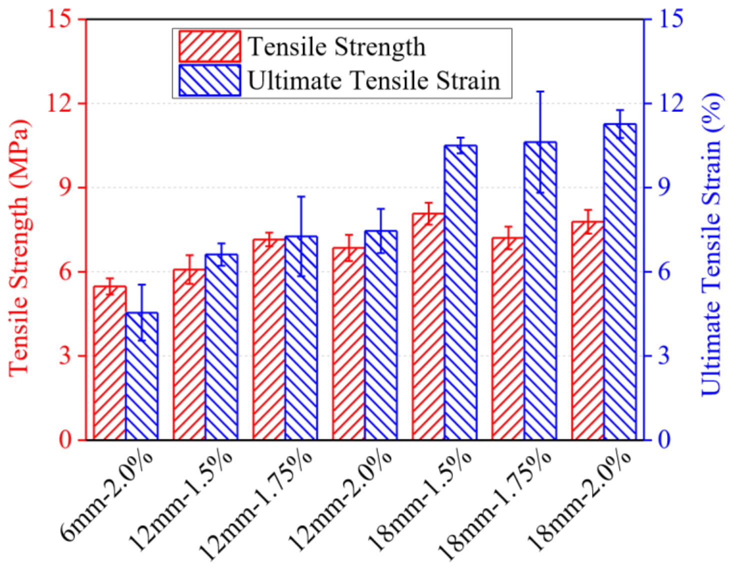

Fig. 9. Comparison of tensile strength and ultimate tensile strain of the EGCs with PE fibres.

Figure 10

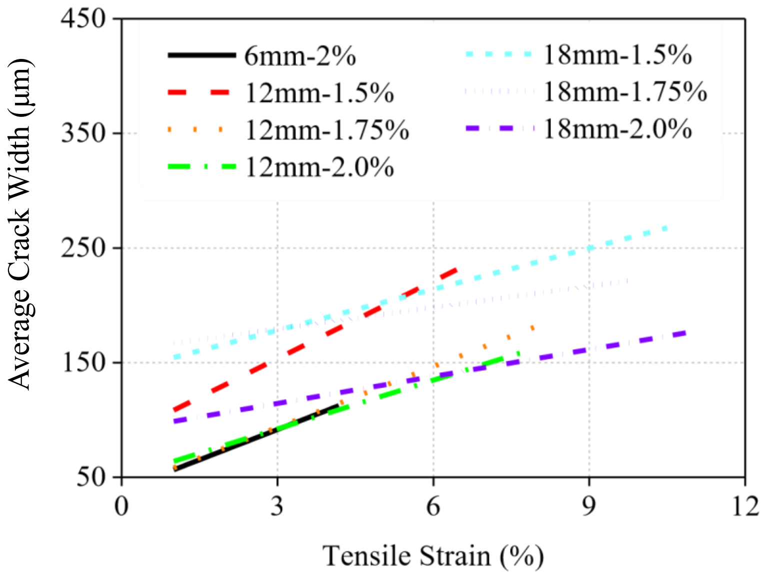

Fig. 10. Linear correlation between the average crack width and corresponding tensile strain levels for the EGCs.

Figure 11

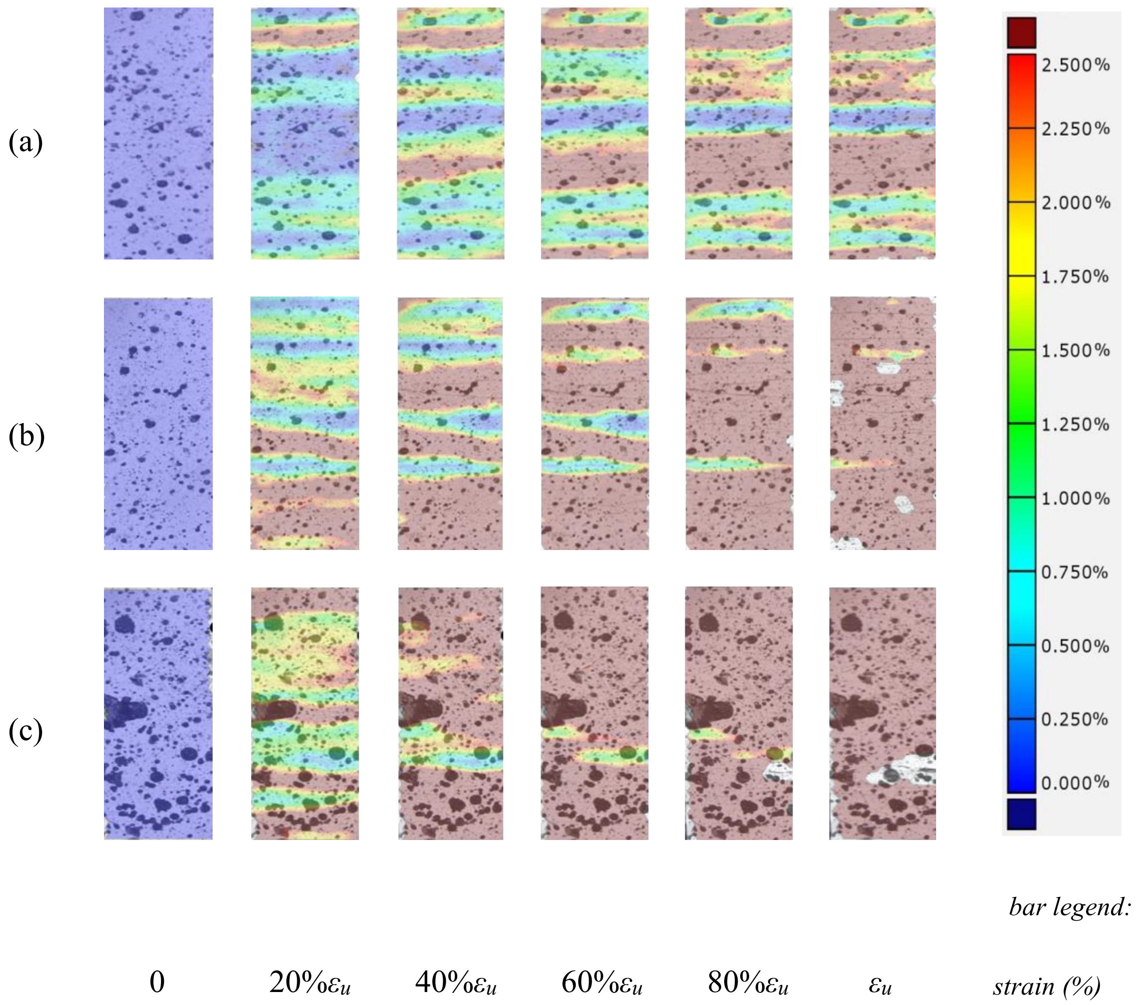

Fig. 11. DIC analysis for the EGCs reinforced by 2% of (a) 6 mm, (b) 12 mm, and (c) 18 mm PE fibres, where the tensile strain increases from ε=0 (left) to $\varepsilon=\varepsilon_u$ (right).

Figure

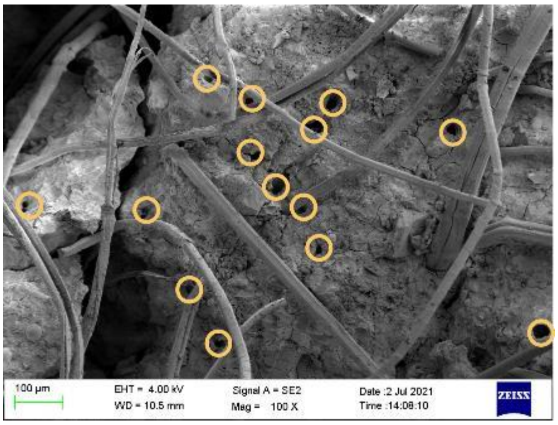

(a)

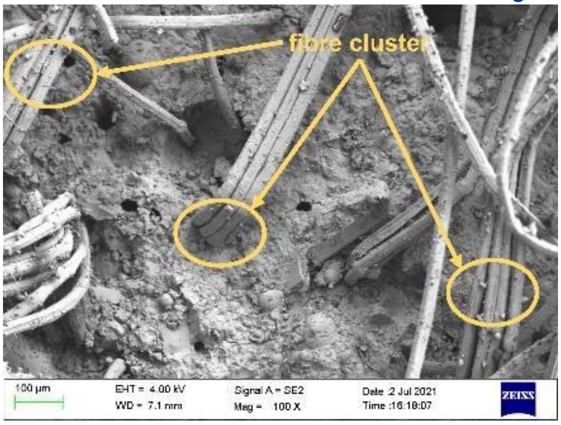

(b)

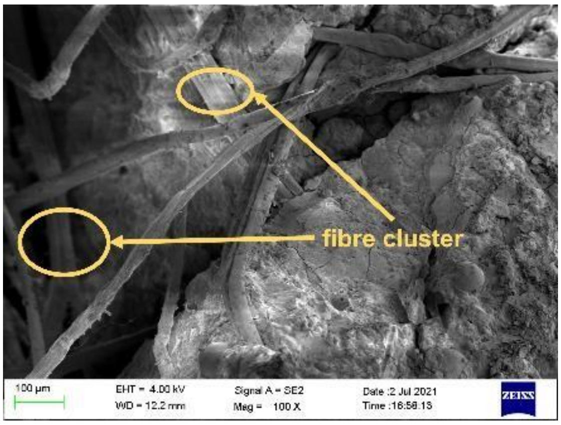

(c)

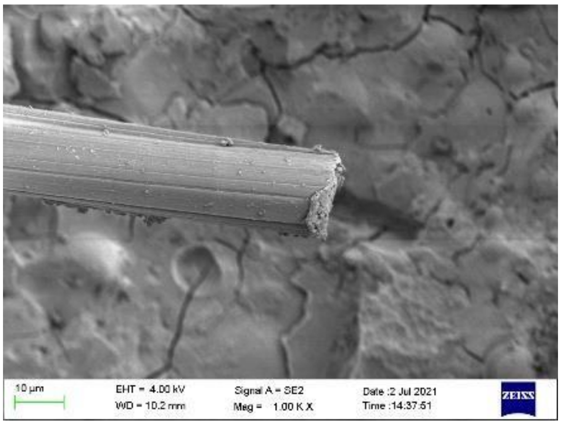

(d)

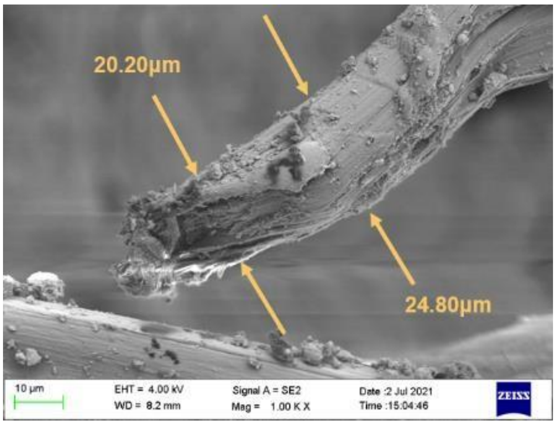

(e)

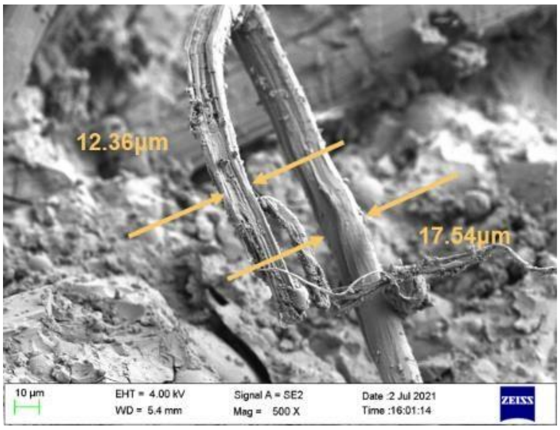

(f)

Fig. 12. SEM images of the cross-sections around the main crack and failure morphology of fibres: (a) PE6-2%-100X, (b) PE12-2%-100X, (c) PE18-2%-100X, (d) PE6-2%-1000X, (e) PE12-2%-1000X, and (f) PE18-2%-500X.

Figure 13

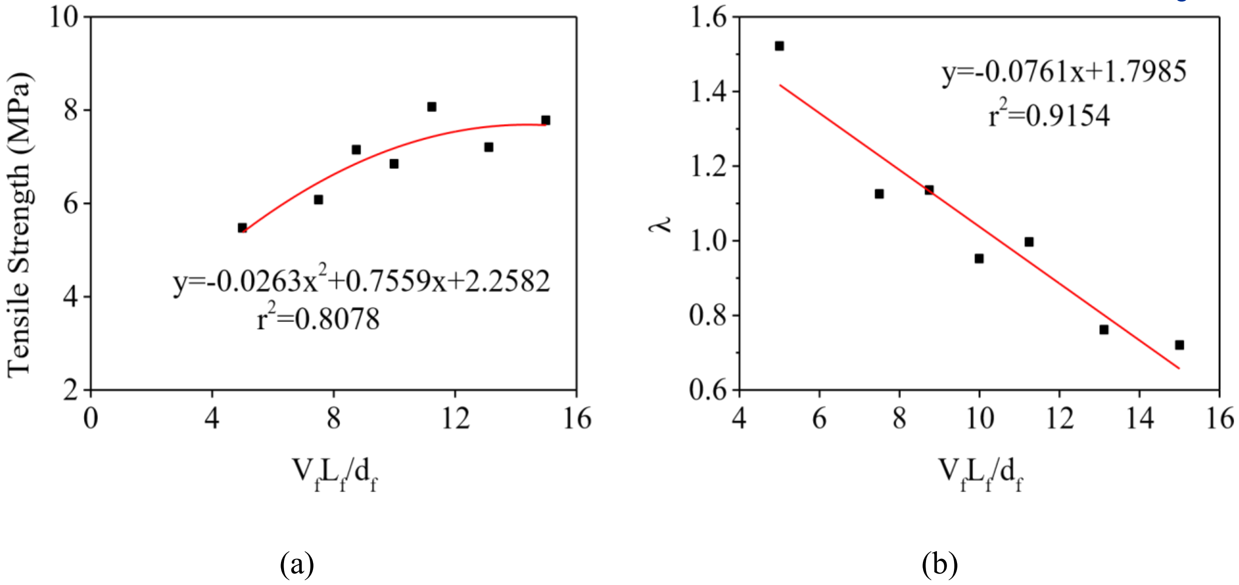

Fig. 13. Relationship between V_fL_f/d_f and (a) tensile strength, and (b) λ.

Figure 14

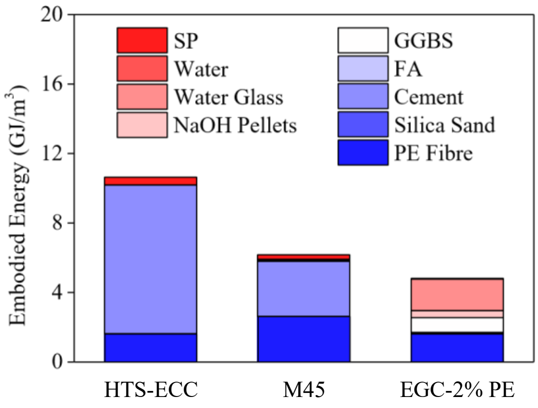

(a)

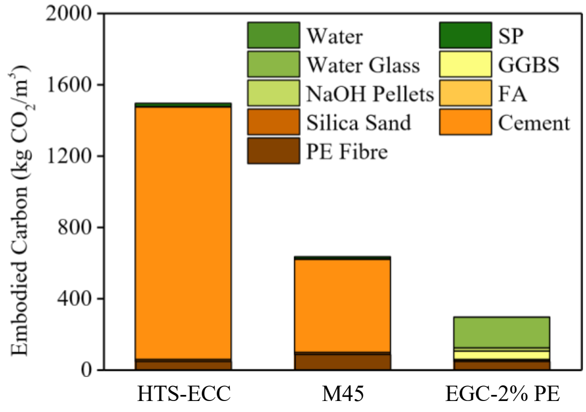

(b)

Fig. 14. (a) Unit-volume embodied energy and (b) Unit-volume embodied carbon of HTS-ECC, M45 ECC and the EGC with 2% of PE fibres.

Response to Comments

* Please check your figure caption list. Each figure that contains parts (a, b, c, etc.) should have these parts labeled in the figure caption list. Please correct.

Response: The figure captions and their list have been revised in the manuscript according to the comment.

* Please ensure your tables are spaced one table per page.

Response: The tables have been spaced one table per page in the manuscript.